On the Synthesis, Microstructure, and Thermoelectric Properties of the Composite Material $Bi_2Te_{2.7}Se_{0.3}/Te_{\delta}$ Obtained from Asymmetric Nanoparticles

M. N. Yapryntsev^{a,*} and M. S. Ozerov^a

*Belgorod State University, Belgorod, Russia
*E-mail: yaprintsev@bsu.edu.ru
Received April 28, 2023; revised May 30, 2023; accepted May 30, 2023

Abstract—Composite materials $Bi_2Te_{2.7}Se_{0.3}/Te_{\delta}$ with varying concentration (δ = 0.15, 0.2, 0.25, and 0.3) are obtained by the solvothermal synthesis of initial powders and their subsequent spark plasma sintering. During the sintering process, the samples are textured, as a result of which lamellar grains are arranged in layers perpendicular to the direction of the application of pressure during sintering (the direction of the texture axis). Upon magnification, the concentration of superstoichiometric tellurium decreases the degree of texturing. The concentration of tellurium does not affect the average grain size. Superstoichiometric tellurium is distributed along the grain boundaries, as a result of which a structure characteristic of composite materials is formed. The release of tellurium at the grain boundaries leads to a change in the thermoelectric properties of the obtained materials. The electrical resistivity naturally increases, and the total thermal conductivity decreases with an increase in the concentration of superstoichiometric tellurium.

Keywords: thermoelectric materials, crystallographic texture, microstructure, spark plasma sintering

DOI: 10.1134/S1063782624700027

1. INTRODUCTION

Thermoelectric phenomena, which provide the direct conversion of thermal and electrical energies, have recently attracted much attention. In accordance with the Ioffe equation, the efficiency of thermoelectric materials is determined by the dimensionless thermoelectric figure of merit $ZT = TS^2/\rho \kappa$, where S is the Seebeck coefficient, p is the electrical resistivity, T is the temperature, and κ is the total thermal conductivity, which is determined by the contributions of charge carriers $(k_e; k_e = (LT)/\rho, L)$ is the Lorentz coefficient) and the crystal lattice (phonons) (κ_p). [1] The electrical resistivity is determined by both the concentration (n) and mobility (u) of charge carriers. A major challenge in creating high-performance thermoelectric materials is the strong coupling between the electrical and thermal transport properties. There are several effective strategies for decoupling properties, such as carrier-concentration optimization, band convergence, phonon scattering, and carrier energy filtering [2]. The use of these approaches in a number of works made it possible to improve the electrical properties of materials or reduce their thermal conductivity, which led to a noticeable improvement in ZT[2]. Also, these approaches can be implemented in various composite thermoelectric materials [3].

Bismuth-telluride solid solutions are the best commercial low-temperature materials. The classical, industrial method of obtaining both p- and n-type solid solutions based on Bi₂Te₃ is zone melting [2]. However, materials obtained by this method have low mechanical properties and delaminate along the bonding planes (001). To solve this problem, powdermetallurgy methods have recently become widespread, in which powdered materials (including nanoscale ones) are produced in various ways and then compacted by hot pressing or spark plasma sintering (SPS). Solvothermal synthesis makes it possible to synthesize bismuth-telluride particles with a controlled size and morphology [4], and the SPS method in some cases makes it possible to preserve the nanostructure, which in turn helps to reduce the lattice contribution to thermal conductivity.

Thus, the combination of methods of solvothermal synthesis and spark plasma sintering potentially makes it possible to obtain composite, nanostructured materials in which mechanisms for optimizing the thermoelectric figure of merit are implemented.

2. EXPERIMENTAL

High-purity bismuth-nitrate pentahydrate $(Bi(NO_3)_3 \cdot 5H_2O, Technical Specification (TU)$

6-09-2230-77), tellurium dioxide (TeO₂, high purity, TU 6-09-1401-76), selenium dioxide (SeO₂, pure, TU 6-09-1338-76), sodium hydroxide (NaOH, chemically pure, State Standard (GOST) 4328-77), isopropanol (GOST 9805-84), acetone (analytical grade, GOST 2603-79) and ethylene glycol (highest grade, GOST 19710-83) were used without further purification.

2.1. Synthesis of Bi₂Te_{2.7}Se_{0.3}

In the typical synthesis procedure, the initial materials per 150 g Bi₂Te_{2.7}Se_{0.3} in a stoichiometric ratio were dissolved in 2000 mL of ethylene glycol in a 3000-mL Erlenmeyer flask by stirring with a magnetic stirrer at a temperature of 100–110°C for 60 min. Then the temperature was increased to 185°C. During heating and when the temperature reached 140–150°C, the color of the solution gradually changed from slightly brown to black. The reaction mixture was kept at 185°C for 6 h. The solution was then cooled to room temperature. Next, the solid product was collected by centrifugation. The powdered material was separated from the solution, redispersed in isopropyl alcohol, followed by treatment in an ultrasonic bath for 15 min. The resulting suspension was subjected to slow centrifugation (4000 rpm, 5 min). The procedure was repeated until the pH of the solution was neutral. The above operation was repeated twice, but isopropyl alcohol was replaced with acetone. The resulting powdered material was dried at room temperature in an air atmosphere for 12 h. This synthesis protocol was optimized to produce 150 g of powder per batch, which was the amount needed to fully characterize and study the thermoelectric properties of a series of 4 samples in two mutually perpendicular directions.

2.2. Te synthesis

In the typical synthesis of tellurium particles, 0.1 mol TeO2 and 20 g of NaOH were dissolved in 1000 mL of ethylene glycol in a 2000-mL Erlenmeyer flask by stirring with a magnetic stirrer at a temperature of 100–110°C for 60 min. Then the temperature was increased to 185°C. When the temperature reached 140–150°C, the color of the solution gradually changed from slightly brown to black. The reaction mixture was kept at 185°C for 2 h. After this time, the solution was cooled to room temperature. The procedure for separating, purifying, and drying the Te powder was similar to the purification procedure Bi₂Te_{2.7}Se_{0.3}. The resulting amount of powdered tellurium turned out to be sufficient for its characterization and obtaining a series of samples of Bi₂Te_{2.7}Se_{0.3}/Te_δ $(\delta = 0.15, 0.2, 0.25, \text{ and } 0.3).$

2.3. Preparation of $Bi_2Te_{2.7}Se_{0.3}/Te_{\delta}$ Powder Mixtures $(\delta = 0.15, 0.2, 0.25, and 0.3)$

The initial powders of $Bi_2Te_{2.7}Se_{0.3}$ and Te in the required ratio (weight ≈ 30 g) were placed in a 250-mL polypropylene container, 200 mL of acetone was added, and then dispersed using a magnetic stirrer (500 rpm) for 2 h. At the end of stirring, the acetone was removed by centrifugation, and the resulting powder was dried at room temperature in an air atmosphere for 12 h.

2.4. Consolidation of the Composite Materials

Dried materials of the composition $Bi_2Te_{2.7}Se_{0.3}/Te_{\delta}$ ($\delta=0.15,\ 0.2,\ 0.25,\ and\ 0.3$) in powder form were loaded into a graphite matrix and compacted into cylinders (20 mm \times 12 mm) using the SPS method. The SPS process was carried out using the SPS Model 10-3 installation (Thermal Technology LLC) at a pressure of 40 MPa and a temperature of 680 K for 2 min in vacuum (0.8 Pa).

2.5. Characterization

The Archimedes method was used to measure the density of samples using an ASP 3.1 device (OOO Porotekh). To determine the crystal structure and phase composition of the initial powders and corresponding bulk samples, X-ray phase analysis (XPA) was employed using a SmartLab diffractometer (Rigaku) with CuK_{α} radiation ($\lambda(CuK_{\alpha}) = 0.15418$ nm, an angular range of 5-80 20, speed of 3°/min, an angular step of 0.01 θ , and a power of 4 kW (40 kV, 100 mA)). To refine the experimental XRD data using the Rietveld method, PDXL software (Rigaku) was used. To calculate the unit-cell parameters, the internal standard method was used. A standard sample of polycrystalline silicon was used as the internal standard (angular range of 5–80 2 θ , speed of 1°/min, and angular step of 0.005θ). To analyze the morphology of particles in the initial powders, estimate the average particle size, and study the characteristics of the grain structure in bulk samples, scanning electron microscopy (SEM) was applied using a Quanta 600 FEG microscope (FEI) (high voltage of 30 kV; working distance of 10 mm). Energy dispersive X-ray spectroscopy (EDX) using Octane Elect EDS for SEM (EDAX Inc.) was employed to map the distribution of chemical elements. The characteristic lines Bi-L, Te-L, and Se-K were used to construct the maps.

To determine the quantitative elemental composition of the bulk samples, an ICPE-9000 inductively coupled plasma optical-emission spectrometer (Shimadzu) was used. For each sample, 3 parallel measurements were carried out.

2.6. Measurement of the Thermoelectric Properties

The Seebeck coefficients were measured using the static direct current method. Electrical-resistivity data were obtained using the standard four-probe method. The Seebeck coefficient and electrical resistivity were measured simultaneously using a ZEM-3 system (ULVAC Advance-Riko) at room temperature under a helium atmosphere. Taking into account the accuracy of the measuring system and the accuracy of the measurements, the error was estimated to be about 4% for the Seebeck-coefficient measurement and 1% for the electrical-conductivity measurement. The total thermal conductivity was calculated as $k = \alpha C_p d$, where α is the thermal diffusivity, $C_{\rm p}$ is the heat capacity, and d is the density of the sample. A TC-1200RH thermal-constant measurement system (ULVAC Advance-Riko) was used to determine the thermal diffusivity (α) of the samples with an estimated error of about 5%. The heat capacity (C_p) calculated from empirical formulas, i.e., $C_p(Bi_2Te_3) = 108.06 +$ $5.53 \times 10^{-2} T \text{ J K}^{-1} \text{ mol}^{-1} \text{ and } C_p(\text{Bi}_2\text{Se}_3) = 118.61 +$ $1.92 \times 10^{-2} T$ J K⁻¹ mole⁻¹, respectively [5] C_p for $Bi_2Te_{2.7}Se_{0.3}$ was estimated as $C_p = [2.7C_p(Bi_2Te_3) +$ $0.3C_{\rm p}({\rm Bi}_2{\rm Se}_3)]/3$. The concentrations (n) and mobility (u) of charge carriers at room temperature (300 K) were measured using a physical-properties measurement system (Cryogenic Ltd) in a magnetic field of 1 T. The values presented correspond to the average of five measurements.

3. RESULTS AND DISCUSSION

The polyol synthesis method allows precise control of the composition of solid solutions in the system $Bi_2Te_{3-x}Se_x$, the content of chalcogens can be adjusted by changing the initial ratios of Se and Te precursors [6, 7]. Since the presence of excess tellurium and free tellurium at the initial stages of synthesis has a significant impact on the morphology of the synthesized particles [8-10], and as a consequence the crystallographic texture, microstructure, and anisotropy of the properties of bulk samples, the composition Bi₂Te_{2.7}Se_{0.3} was synthesized in a separate process in the necessary quantity to obtain a series of samples (Bi₂Te_{2.7}Se_{0.3} /Te_{δ} (δ = 0.15, 0.2, 0.25, and 0.3)). Tellurium particles were produced in a separate process, and then the powdered materials were combined in the required ratio and sintered using the SPS method. The synthesis protocols for the production of Bi₂Te_{2.7}Se_{0.3} and Te, including the purification steps, were characterized by material yields above 98%. A SEM image of Bi₂Te_{2.7}Se_{0.3} particles is shown in Fig. 1a. According to Fig. 1a, the particles had an average diameter (d) of 314 ± 130 nm and an average thickness (h) of 46 ± 10 nm (Figs. 1b and 1c)). The particlesize distribution for all samples in this work was described using a lognormal unimodal distribution function.

According to XRD, the initial $Bi_2Te_{2.7}Se_{0.3}$ powder is single phase and represents the rhombohedral phase $R\overline{3}m$, which is typical for pure Bi_2Te_3 (JCPDS no. 01-089-2009). The XRD results for the initial powder are shown in Fig. 1d. The lattice parameters a, b, and c are equal to 4.377 and 30.443 Å, respectively.

Figure 2a shows a SEM image of "rice-like" Te particles, with an average length (*l*) of $4.7 \pm 1.6 \,\mu m$ and average diameter (*d*) of $1.6 \pm 0.3 \,\mu m$ (Figs. 2b and 2c).

According to XRD (Fig. 2d), the initial Te powder is single phase with the trigonal phase P3121, which is characteristic of Te (JCPDS no. 01-079-0736). The calculated lattice parameters a, b, and c are equal to 4.462 Å and 5.931 Å, respectively.

Next, powder mixtures of $Bi_2Te_{2,7}Se_{0,3}Te_{\delta}$ ($\delta=0.15,\ 0.2,\ 0.25,\ and\ 0.3$) were prepared. The resulting powder mixtures were subjected to SPS. Measured by the Archimedes method, the relative densities of the resulting materials did not depend on δ and amounted to about $\approx 98\%$, relative to the density of $Bi_2Te_{2,7}Se_{0,3}$. The X-ray diffraction of bulk samples in two perpendicular directions relative to the pressing direction demonstrated that the consolidated material is characterized by the presence of a crystallographic texture, with the [001] direction oriented along the pressing axis (Fig. 3).

The X-ray diffraction patterns are shown in Figs. 3a and 3b. Like the diffraction patterns for the initial Bi₂Te_{2.7}Se_{0.3} powder, all diffraction patterns for bulk samples also correspond to the space symmetry group R3m. The crystallographic symmetry of the samples under study and the crystal-lattice parameters do not depend on δ. According to the XRD results, all bulk materials are two phase (contain Te). The lattice parameters a and c calculated by the internal standard method for all samples were equal to 4.375 and 30.343 Å, respectively. Since tellurium evaporation is inevitable during SPS [11], the actual composition of the samples may deviate from the nominal one. The evaporation of tellurium for materials based on bismuth telluride was described in [11]. This effect was also observed in our experiment. In contrast to Te, the contents of Bi and Se turned out to be almost δ independent, i.e., changes in the stoichiometric composition due to evaporation observed in the samples should be attributed to changes in the Te content. The dependence of the Te content on δ is given in Table 1. It can be seen that the Te content naturally increases with increasing δ , but the experimental and theoretical values of δ are very different.

To study the microstructure of the obtained samples, the chipped surfaces were examined using the SEM method (the chipped surfaces were oriented per-

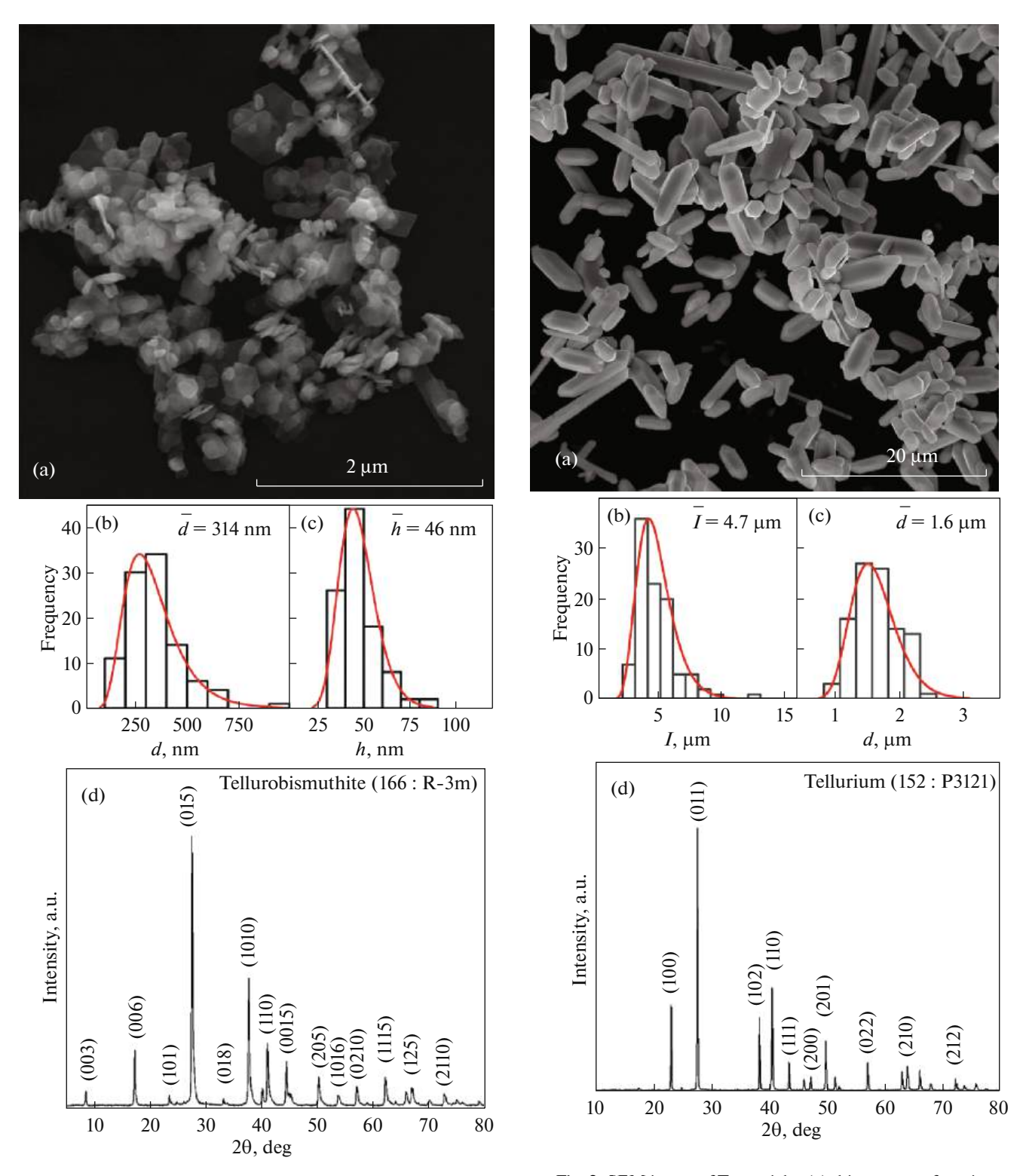


Fig. 1. SEM image of Bi₂Te_{2.7}Se_{0.3} particles (a), histograms of the particle distribution by diameter and thickness, (b, c) and the X-ray diffraction pattern (d), respectively.

Fig. 2. SEM image of Te particles (a), histograms of particle distribution by length and diameter, (b, c) and the X-ray diffraction pattern (d), respectively.

pendicular and parallel to the direction of the application of pressure). Figure 4 shows SEM images of chips for samples with $\delta = 0.15$ and 0.30, which are oriented perpendicular and parallel to the pressing direction.

It can be seen that the crystallographic texture detected by XRD is also observed in the SEM images. Individual grains are characterized by a morphology close to lamellar. The stacking and recrystallization of

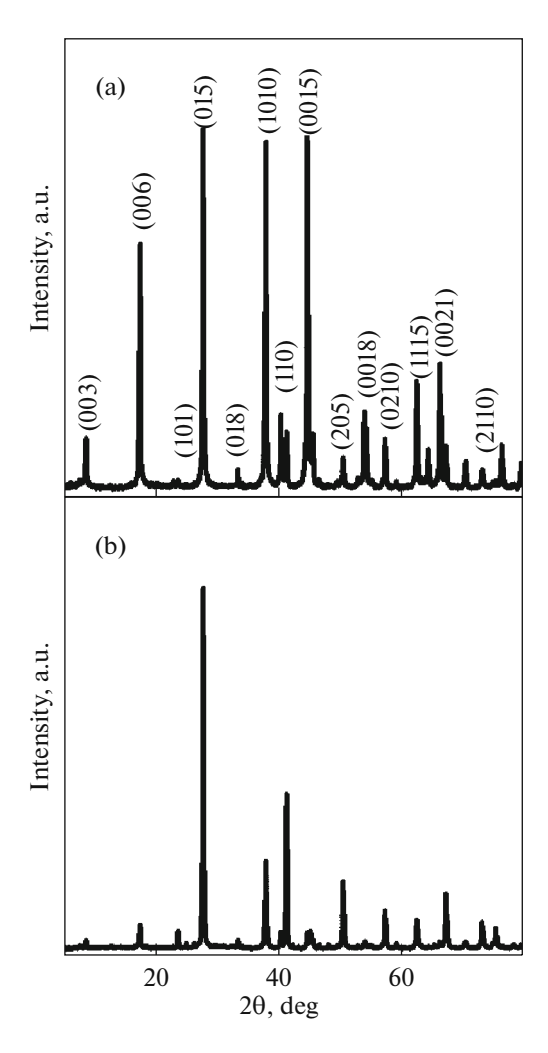


Fig. 3. Diffraction pattern for $Bi_2Te_{2.7}Se_{0.3}/Te_{0.15}$ taken on perpendicular (a) and parallel (b) surfaces relative to the direction of pressing.

particles of the initial powder leads to the formation of a lamellar structure [12–14]. For all obtained samples, the average values of the diameter (D) and thickness (H) were calculated. The calculated average values $D=1.55~\mu m$ and $H=0.25~\mu m$ were δ independent. It can be noted that for the sample with $\delta=0.15$, the degree of grain ordering is higher (Figs. 4c and 4d).

To quantify the degree of texturing for all samples, the Lotgering factor (LF) was calculated by analyzing the XRD results in accordance with the methodology given in [15].

The dependence of the LF on δ is given in Table 1; the LF decreases as δ increases. The development of crystallographic texture in Bi₂Te₃-based materials is determined by two main factors: the recrystallization process and the rotation of grains along the basal plane [16]. It is known [16] that the initial stage of the SPS process is the packing of particles of the initial powder under external pressure. During the packing process, the restructuring of randomly oriented lamellar parti-

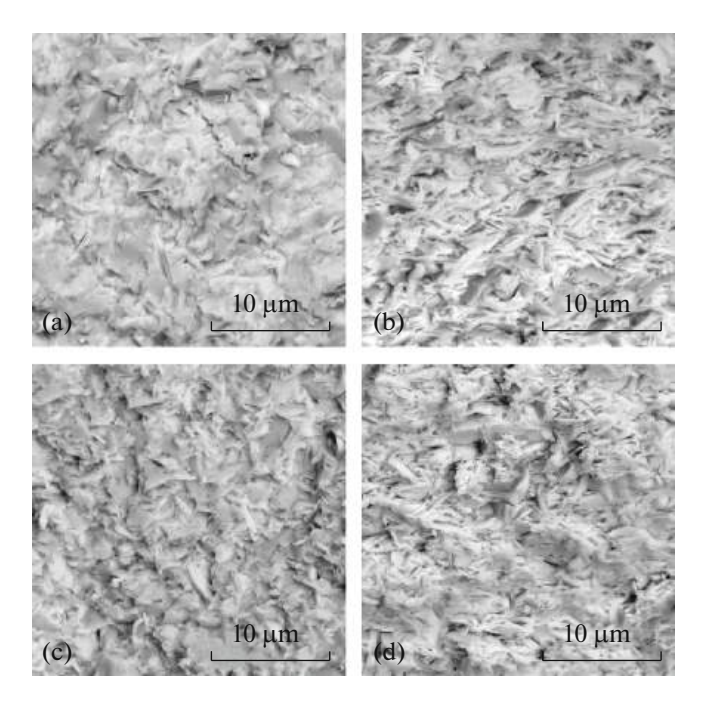


Fig. 4. SEM image of chipped samples surfaces with δ = 0.15 (a, b) and 0.30 (c, d), which are oriented perpendicular to (a, c) and parallel to (b, d) the direction of pressing.

cles occurs, which leads to the formation of crystallographic texture. Some nanoscale powdery inclusions can act as a "lubricant" to help the particles rotate as they pack during the SPS process. Thus, a number of works reported the effect of Ce in Al₂O₃ as a lubricant [17] or Te lubricant in Bi₂Te₃ [18]. Increasing the Te content should lead to more efficient particle packing and a corresponding increase in the preferred grain orientation, as a result the LF should gradually increase. Considering that D and H turned out to be δ independent, i.e., the concentration of excess tellurium does not affect recrystallization during the SPS process with given parameters (40 MPa, 680 K and 2 min); the main mechanism for the development of crystallographic texture is the process of grain rotation [19]. The LF(δ) dependence is determined by the rotation process. Establishing the mechanism of texture formation in the samples under study requires more detailed experimental study. Available data sug-

Table 1. Quantitative elemental composition (relative to Bi = 2), crystal-lattice parameters, and anisotropy coefficient (Lotgering Factor)

δ	C(Te), at %	C(Se), at %	a = b, Å	c, Å	LF
0.15	54.76	6.04	4.355	30.329	0.29
0.20	55.42	6.05	4.358	30.332	0.22
0.25	56.59	6.04	4.361	30.338	0.18
0.30	57.27	6.06	4.368	30.371	0.13

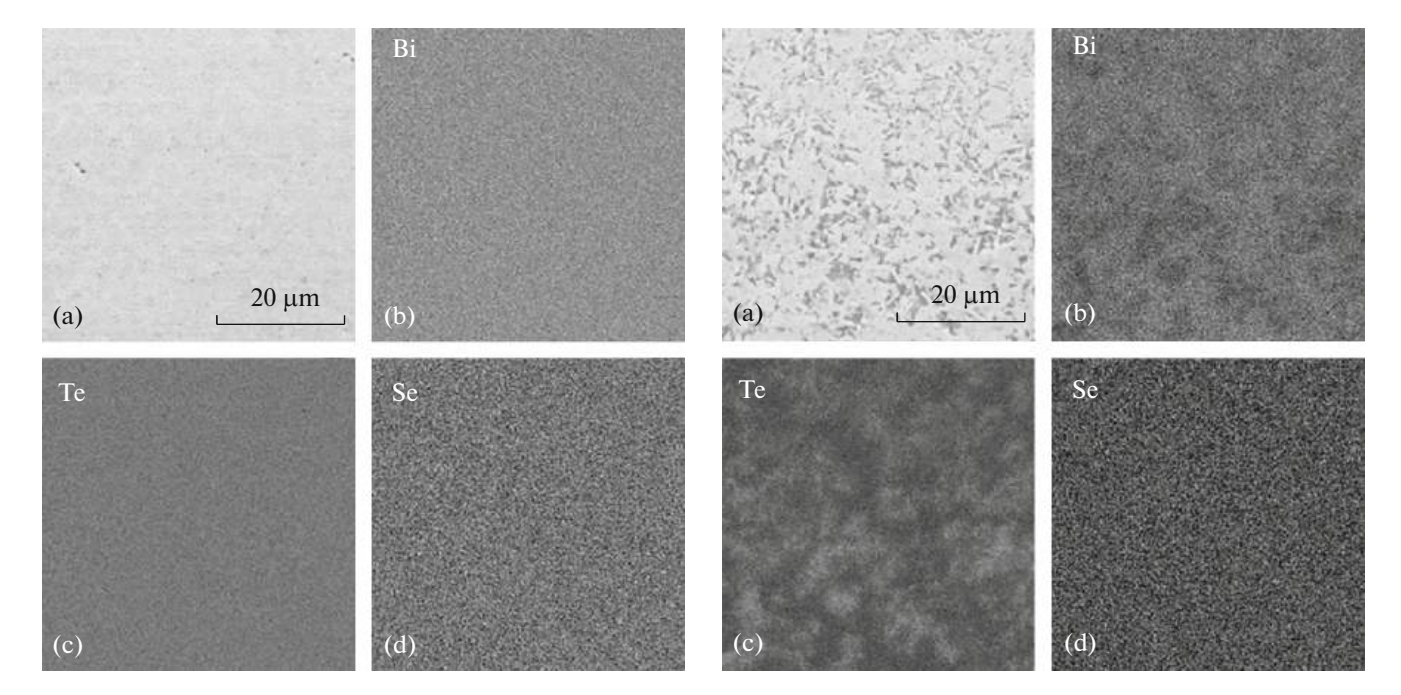


Fig. 5. Distribution maps of Bi, Sm, Te, and Se for the sample with $\delta = 0.15$.

Fig. 6. Distribution maps of Bi, Sm, Te, and Se for the sample with $\delta = 0.30$.

gest that with increasing δ and given SPS-process parameters (40 MPa, 680 K and 2 min), rotation may be difficult. Works [19, 20] demonstrate the production of highly textured samples based on bismuth telluride with an excess of tellurium. However, in these works, the development of crystallographic texture is accompanied by the removal of excess tellurium in the form of a melt when a dynamic load is applied, which stimulates the rotation process. In our work, due to the short pressing time and relatively low temperature (below the melting point of tellurium), the removal of tellurium in the form of a melt is impossible, which is why the precipitation of a secondary tellurium phase at the grain boundaries in an amount exceeding a certain threshold value may cause inhibition of the process of particle rotation along the basal plane and as a consequence, a decrease in the LF.

To study the distribution of chemical elements in bulk samples, EDX maps of the distributions of Bi, Te, and Se were constructed for the polished surfaces of Bi₂Te_{2.7}Se_{0.3}Te_{δ} (δ = 0.15 and 0.3) samples. For the sample with δ = 0.15, all elements were evenly distributed over the surfaces, due to the low concentration of superstoichiometric tellurium (0.76 at %), the presence of a second phase is not observed. Maps for the sample with δ = 0.15 are shown in Fig. 5. For the sample with δ = 0.3, an uneven distribution of tellurium on the polished surface of the sample is observed. The darker areas in the SEM image (Fig. 6a) correspond to areas with a high tellurium content and depressions formed during vibration polishing. The formation of a developed surface relief is a consequence of the chip-

ping of individual grains or their fragments; therefore, the high tellurium content in these areas indicates the release of tellurium at the grain boundaries and the formation of a structure characteristic of composite materials. Maps for a sample with $\delta=0.3$ are shown in Fig. 6.

The release of tellurium at the grain boundaries and the formation of a microstructure characteristic of a composite material has a significant impact on the thermoelectric properties. Therefore, the thermoelectric properties of the resulting series of samples were further studied at room temperature.

The thermoelectric figure of merit is determined by a combination of the electrical resistivity, Seebeck coefficient, and total thermal conductivity. Figure 7a shows the dependence of the electrical resistivity on the tellurium concentration at room temperature measured in the direction perpendicular and parallel to the pressing direction. Regardless of the direction of measurement, the electrical resistivity depends on the tellurium concentration; increasing the tellurium concentration leads to an increase in the electrical resistivity. This trend may be associated with changes in the concentration of the main charge carriers and their mobility. The *n* values are practically independent of δ and equal to 2.5×10^{19} cm⁻³. While the carrier mobility decreases linearly with increasing δ , there is a change in both directions. For the perpendicular measurement orientation, the mobility decreases from 461 up to 237 cm⁻³ for samples with $\delta = 0.15$ and 0.30, respectively. And for the parallel measurement orientation, the mobility decreases from 133 up to 81 cm⁻³

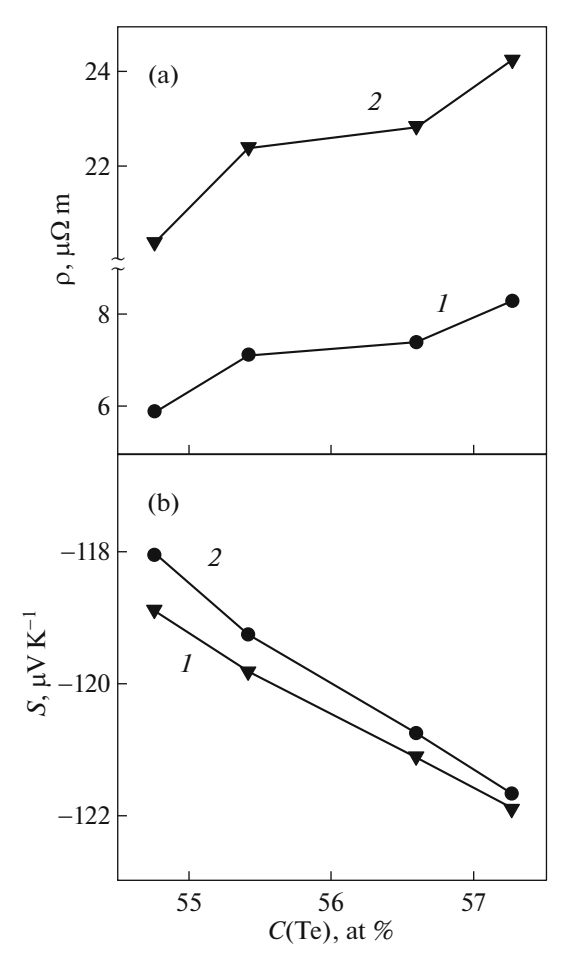


Fig. 7. Dependence of the electrical resistivity (a) and the Seebeck coefficient (b) at room temperature on the concentration of tellurium, measured in the direction perpendicular to (1) and parallel to (2) the direction of pressing.

for samples with $\delta=0.15$ and 0.30, respectively. As is known, the presence and concentration of point defects in bismuth telluride determines the type and concentration of the main charge carriers [21–23]. The fact that the charge-carrier concentration does not change with increasing δ indicates that free tellurium evaporates first, and the chemical composition of the matrix $Bi_2Te_{2.7}Se_{0.3}$ remains constant. The change in the mobility of charge carriers is due to their additional scattering at the interface. Thus, the increase in the electrical resistivity with increasing δ is determined by a decrease in the mobility of charge carriers.

Figure 7b shows the dependence of the Seebeck coefficient on the tellurium concentration at room temperature measured in the direction perpendicular and parallel to the pressing direction. The sign of the Seebeck coefficient is negative. The Seebeck coefficient in materials based on bismuth telluride is a weakly anisotropic value; the values of the Seebeck coefficient for both orientations are close. It is known

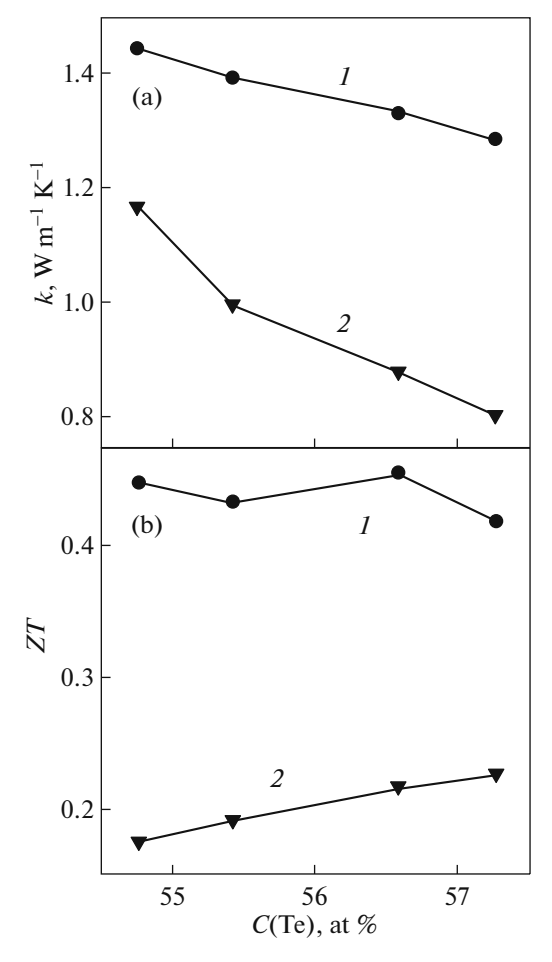


Fig. 8. Dependence of the total thermal conductivity (a) and the thermoelectric figure of merit (b) at room temperature on the concentration of tellurium, measured in the direction perpendicular to (1) and parallel to (2) the direction of pressing.

that the Seebeck coefficient of a degenerate semiconductor can be described in accordance with expression (1).

$$S = \frac{2k_{\rm B}^2 T m^*}{3e\hbar^2} \left(\frac{\pi}{3n}\right)^{2/3} \tag{1}$$

where $k_{\rm B}$ is the Boltzmann constant, T is the absolute temperature, e is the elementary charge, \hbar is the reduced Planck's constant, and n is the charge-carrier concentration [24, 25].

From this expression it can be noted that the Seebeck coefficient is inversely proportional to the concentration of charge carriers. Considering the fact that the charge-carrier concentration does not change as δ changes, we can conclude that n is not the determining factor in the change in the values of the Seebeck coefficient. It was shown in [26] that the change in m^* is inversely proportional to the mobility of charge carriers, which will also explain the slight anisotropy of the Seebeck coefficient (Fig. 8b). Thus, an increase in δ leads to a decrease in μ and, as a consequence, an

increase in m^* , which in turn leads to an increase in the modulus of the Seebeck coefficient.

The dependences of the total thermal conductivity on the tellurium concentration at room temperature measured in the direction perpendicular and parallel to the pressing direction are shown in Fig. 8a. It has been found that the thermal conductivity for the perpendicular orientation, regardless of the tellurium concentration, is much higher than for the parallel orientation. The k(C(T)) dependences for all studied samples, measured in the direction perpendicular and parallel to the pressing direction, correlate with the values of the electrical resistivity, which indicates the influence of the contribution of charge carriers to the overall thermal conductivity. It should also be noted that the precipitation of tellurium at the grain boundaries leads to additional scattering of phonons at the phase boundary. The change in the total thermal conductivity at room temperature depending on the content of superstoichiometric tellurium is determined by both the change in the contribution of charge carriers and the photon contribution to the total thermal conductivity of the materials under study. The significant difference in the total thermal conductivity measured in two mutually perpendicular directions relative to the pressing axis is determined by the anisotropy of the microstructure and crystallographic texture of the obtained samples.

The electrical transport (ρ, S) and thermal properties (k) are determined by the formation of a specific defect structure, the precipitation of superstoichiometric tellurium at the grain boundaries, and the crystallographic anisotropy of the resulting materials.

The dependences of the thermoelectric figure of merit on the tellurium concentration at room temperature measured in the direction perpendicular and parallel to the pressing direction are shown in Fig. 8b.

The highest ZT value is achieved for samples measured in the direction perpendicular to the pressing axis and these values are practically independent of the concentration of superstoichiometric tellurium: the positive effect of a decrease in the thermal conductivity is completely offset by an increase in electrical resistivity. For the parallel measurement direction relative to the pressing direction, an increase in ZT is observed with increasing concentration of superstoichiometric tellurium. This is due to an intense decrease in the thermal conductivity with increasing tellurium concentration as a result of intensified phonon scattering at the interface with increasing tellurium content. The fact that all thermoelectric figureof-merit values measured in the direction perpendicular to the extrusion direction are significantly higher relative to the parallel extrusion direction shows that in addition to alloying and defect engineering (a change in the tellurium concentration), texture control can be considered as a promising way to optimize the thermoelectric properties.

4. CONCLUSIONS

It has been established that with an increase in the concentration of superstoichiometric tellurium in the samples under study, a structure characteristic of composite materials is formed; tellurium is precipitated as a separate phase at the grain boundaries.

The concentration of superstoichiometric tellurium does not affect the average grain size in bulk materials, but does affect the degree of the preferential orientation of individual grains and the formation of crystallographic texture.

The concentration of superstoichiometric tellurium is related to the thermoelectric properties of the resulting materials. As the tellurium concentration increases, the electrical resistivity and the modulus of the Seebeck coefficient increase with a simultaneous decrease in the overall thermal conductivity. These effects are due to the scattering of charge carriers and phonons at the phase boundaries.

FUNDING

This work was supported by the Russian Science Foundation (grant no. 21-73-00199). The work was carried out using equipment of the Joint Research Center of Belgorod State National Research University "Technology and Materials."

CONFLICT OF INTEREST

The authors of this work declare that they have no conflicts of interest.

REFERENCES

- G. J. Snyder and A. H. Snyder, Energy Environ. Sci. 10, 2280 (2017).
- Y. Liu, Y. Zhang, K. H. Lim, M. Ibáñez, S. Ortega, M. Li, et al., ACS Nano 12, 7174 (2018).
- 3. V. C. Theja, V. Karthikeyan, D. S. Assi, and V. A. Roy, ACS Appl. Electron. Mater. 4, 4781 (2022).
- 4. M. Yaprintsev, A. Vasil'ev, O. Ivanov, D. Popkov, and E. Kudryavtsev, Solid State Sci. **135**, 107083 (2023).
- 5. M. Hong et al., ACS Nano 10, 4719 (2016).
- 6. Q. Fu et al., J. Solid State Chem. **300**, 122188 (2021).
- 7. Y. S. Lim, S. M. Wi, and G. G. Lee, J. Eur. Ceram. Soc. **37**, 3361 (2017).
- J. L. Mi, M. Søndergaard, P. Hald, et al., ACS Nano 4, 2523 (2010).
- 9. W. Wang et al., J. Am. Chem. Soc. 132, 17316 (2010).
- M. Yaprintsev, A. Vasil'ev, and O. Ivanov, J. Eur. Ceram. Soc. 39, 1193 (2019).
- 11. H. Shen et al., Materials, 4204 (2022).
- 12. Q. Lognoné et al., J. Am. Ceram. Soc. 97, 2038 (2014).
- 13. Z. Tang et al., J. Mater. Chem. C 3, 10597 (2015).

- 14. F. K. Lotgering, J. Inorg. Nucl. Chem. 9, 113 (1959).
- 15. L. Wang et al., J. Asian Ceram. Soc. 3, 183 (2015).
- 16. I. Alvarez-Clemares et al., Adv. Eng. Mater. **12**, 1154 (2010).
- 17. Y. Liu et al., ACS Nano 12, 7174 (2018).
- 18. Y. Wu et al., Adv. Sci. 6, 1901702 (2019).
- 19. Y. Liu et al., ACS Nano. 12, 7174 (2018).
- 20. Y. Pan, T. R. Wei, C. F. Wu, and J. F. Li, Mater. Chem. C 3, 10583 (2015).
- 21. L. Hu, T. Zhu, X. Liu, and X. Zhao, Adv. Funct. Mater. **24**, 5211 (2014).
- 22. J. Suh, K. M. Yu, D. Fu, X. Liu, F. Yang, J. Fan, D. J. Smith, Y. H. Zhang, J. K. Furdyna, C. Dames,

- W. Walukiewicz, and J. Wu, Adv. Mater. 27, 3681 (2015).
- 23. S. Chu, Nature (London, U.K.) 488, 294 (2012).
- 24. M. S. Dresselhaus, Nature (London, U.K.) **414**, 332 (2001).
- 25. L. N. Lukyanova, A. A. Shabaldin, A. Y. Samunin, and O. A. Usov, Semiconductors **56**, 10 (2022).

Publisher's Note. Pleiades Publishing remains neutral with regard to jurisdictional claims in published maps and institutional affiliations.

AI tools may have been used in the translation or editing of this article.